Gadolinium doped ceria interlayers for Solid Oxide Fuel Cells cathodes: Enhanced reactivity with sintering aids (Li, Cu, Zn), and improved densification by infiltration

Clément Nicollet, Jenny Waxin, Thomas Dupeyron, Aurelien Flura, Jean-Marc Heintz, Jan Pieter Ouweltjes, Paolo Piccardo, Aline Rougier, Jean-Claude Grenier, Jean-Marc. Bassat

Gadolinium doped ceria interlayers for Solid Oxide Fuel Cells cathodes: enhanced reactivity with sintering aids (Li, Cu, Zn), and improved densification by infiltration

Clement Nicollet[1], Jenny Waxin[1], Thomas Dupeyron[1], Aurélien Flura[1], Jean-Marc Heintz[1], Jan Pieter Ouweltjes[2], Paolo Piccardo[3], Aline Rougier[1], Jean-Claude Grenier[1], Jean-Marc Bassat[1]

[1] CNRS, Univ. Bordeaux, ICMCB, UPR 9048, F-33600 Pessac, France
[2] HTceramix SA, Avenue des Sports 26, Yverdon-les-Bains, Switzerland
[3] Laboratory of Metallurgy and Materials, Department of Chemistry and Industrial Chemistry, University of Genoa, Genoa, 16146, Italy

Abstract:

This paper reports the study of the densification of 20 % Gd doped ceria (GDC) interlayers in SOFC cathodes through two different routes: the well-known addition of sintering elements, and an innovative densification process by infiltration. First, Li, Cu, and Zn nitrates were added to GDC powders. The effect of these additives on the densification was studied by dilatometry on pellets, and show a large decrease of the sintering temperature from 1330 °C (pure GDC), down to 1080 °C, 950 °C, and 930 °C for Zn, Cu, and Li addition, respectively. However, this promising result does not apply to screen-printed layers, which are more porous than pellets and in which the shrinkage is constrained by the substrate. The second approach consists in preparing a pre-sintered GDC layer, which is subsequently infiltrated with Ce and Gd nitrates and sintered at 1250 °C to increase its density. Such an approach results in highly dense GDC interlayers. Using $La_{0.6}Sr_{0.4}Co_{0.2}Fe_{0.8}O_{3-\delta}$ (LSCF) as electrode, the influence of the interlayers on the cathode performance was studied. The addition of sintering aids dramatically increases the cell resistances, most likely because the additives increase the reactivity between GDC and either Yttria Stabilized Zirconia (YSZ) or LSCF, thus losing the expected benefit related to the decrease of sintering temperatures. The interlayers prepared by infiltration do not induce additional resistances in the cell, which results in power densities of single cells 40-50 % higher than those of cells prepared with commercial GDC interlayers, making this approach a valuable alternative to sintering aids.

1 Introduction

Electrochemical devices such as Solid Oxide Fuel Cells (SOFCs) are valuable technologies for energy conversion and storage. Like in every electrochemical system, the interfaces between the electrodes and the electrolyte play a crucial role in the efficiency of the device. $La_{0.6}Sr_{0.4}Co_{0.2}Fe_{0.8}O_{3-\delta}$ (LSCF), widely studied as SOFCs cathode material, *i.e.* where the oxygen reduction takes place, is well known to strongly

reacts with zirconia based electrolytes such as 8 % yttria stabilized zirconia (8YSZ), forming insulating phases namely $La_2Zr_2O_7$ and $SrZrO_3$ [1]. Using a Gd-doped ceria (GDC) interlayer between the LSCF cathode and the YSZ electrolyte is a widespread approach to limit such an issue [2, 3]. To be fully efficient, the GDC interlayer should be dense, as reported by several authors [4-11], because Sr species can easily diffuse on the surface of GDC grains and still react with zirconia if the interlayer is porous [12]. The most common way to prepare GDC interlayers is the screen-printing of a GDC ink followed by a sintering step at high temperature. This last step is critical for the final performance of the cell. On the one hand, a low sintering temperature of GDC produces a porous interlayer, therefore favoring Sr diffusion; on the other hand, high temperature sintering will result in a denser GDC layer that limit Sr diffusion more efficiently [8], but can either favor the diffusion of Gd cations in the YSZ electrolyte [13], or create $(Zr,Y,Ce,Gd)O_X$ solid solution [14, 15], both with low conductivities affecting the cell performance. It is then mandatory to consider strategies for ceria densification that do not involve high temperature sintering. Deposition methods such as spray based [7, 16] or plasma based [2, 3, 5, 17] techniques allow decreasing the final sintering temperature to get dense ceria layers, and generally lead to improved performance and durability. But these techniques are less attractive from an industrial point of view as they imply changes in the steps of the preparation of the cells.

The ideal approach is thus to find an easy and potentially cheap method to densify screen-printed layers at temperature low enough to avoid Ce and Gd diffusion. It is possible with the addition of sintering aids in the GDC powder that can significantly decrease the densification temperature of GDC. Nicholas and De Jonghe [18] compared the effect of many elements (additives) on the densification of GDC, and the highest densification values were obtained with the addition of Li, Zn, Co, and Cu. Most studies on sintering aids for doped-ceria were focused on pellets densification and characterization of their electrical conductivity [19-25], with the aim to build anode supported cells with doped-ceria electrolytes, but few papers addressed the influence of these sintering aids on the electrode performance when used as additives in GDC interlayers. As the Co addition in GDC has been widely studied [26-28], we focused our efforts on the three other candidates, *i.e.* Li, Zn, and Cu.

In the present study, we have evaluated the effect of Li, Zn, and Cu as sintering aids of $Ce_{0.8}Gd_{0.2}O_{1.9}$ interlayers not only on their densification, but also on the electrochemical performance of the LSCF electrode, by studying carefully their influence on both the electrolyte series resistance and the electrode polarization resistance, both being dependent on the characteristics of the GDC interlayer.

As an alternative way of adding the sintering aids, Ni and Esposito used the infiltration route of a Co nitrate solution to pre-sintered GDC interlayers [29]. In this work, we also considered the infiltration as a densification route, but only of Ce and Gd nitrates solution to fill the remaining porosity of the GDC interlayer. This approach, already presented by Choi *et al.* in the case of GDC sol infiltration [30], aims at

improving the interlayer density without changing its composition. The performance obtained with this route is also presented and compared with that obtained using sintering aids.

2 Experimental

This study is focused on the oxygen electrode architecture for fuel cells using 8YSZ electrolytes. The electrode architecture consists of a GDC interlayer and a LSCF electrode. As the GDC interlayer is the core of the study, all other preparation parameters were kept constant.

2.1 Preparation of symmetrical and single cells

Symmetrical cells were all based on commercial 8YSZ membrane (Fuelcellmaterial.com) of 25 mm diameter and 250 µm thickness. Complete single cells were based on commercial anode-electrolyte NiYSZ/YSZ half cells (Elcogen company).

The preparation of the $Ce_{0.8}Gd_{0.2}O_{1.9}$ interlayer is detailed below. The LSCF electrode was prepared by screen printing, starting from a sub-micrometric powder provided by Marion Technologies®. The diameter of the electrode is 14.5 mm and its thickness is approx. 20 µm. The electrodes were sintered at 1050 °C for 1 h for all symmetrical and single cells.

2.2 Preparation of GDC interlayers

As mentioned in the introduction, two ways of preparing the GDC layer were considered in this work: adding a metal oxide to the GDC powder to increase its sinterability, or filling the remaining pores of a pre-sintered screen-printed GDC layer by infiltrating a nitrate solution containing both Ce and Gd cations in the proper ratio. Figure 1 illustrates the different steps related to both preparation methods.

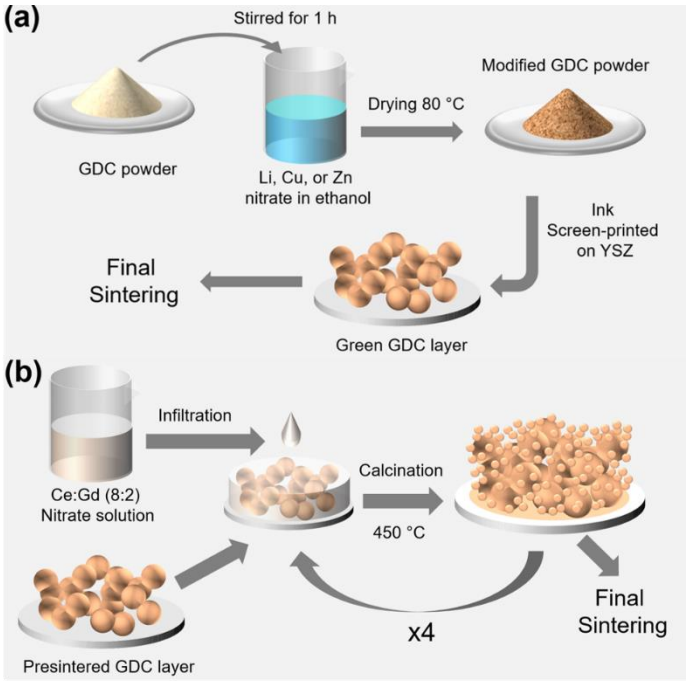

Figure 1 : Illustration of the two preparation methods: (a) addition of sintering aids to the starting GDC powder and (b) infiltration of Ce-Gd nitrates into a pre-sintered GDC layer

2.2.1 Addition of sintering aids

Regarding the amount of sintering aid required to reach the highest densification, Nicholas and De Jonghe [18] reported that no difference is observed in the final relative density of GDC between 3 at. % and 5 at. % of sintering aid. In this study, the amount of sintering aid in GDC was fixed to 3 at. % for the three selected elements (Li, Zn, and Cu).

These elements were added to GDC by dissolving the proper amount of metal nitrates (3 at. %) into alcohol, mixing the solution and the GDC powder with a magnetic stirrer for 1 h and heating at 80 °C until the complete evaporation of the alcohol. Then, the powder was either pressed into green pellet for dilatometry measurements, or prepared as an ink for further screen-printing of the interlayers (Figure 1a). The sintering temperature of the screen-printed layer is a key parameter, and is discussed in the results section.

2.2.2 Infiltration process

The densification by the infiltration route is illustrated in Figure 1b. A $Ce_{0.8}Gd_{0.2}O_{1.9}$ (GDC) layer was first prepared by screen-printing, then pre-sintered at moderate temperature as detailed below. The final density of the layer increases when decreasing the pre-sintering temperature, but the layer has to be mechanically strong enough to withstand subsequent infiltration steps. Thus, a compromise has to be found. After optimization, the pre-sintering temperature was fixed to 1150 °C for 1 h. Secondly, a solution of cerium and gadolinium was prepared by dissolving $Ce(NO_3)_3;6H_2O$ and $Gd(NO_3)_3;6H_2O$ nitrates (Aldrich)

with the proper stoichiometry (8:2) in water. The screen-printed layers were then infiltrated with the nitrate solution, and the infiltrated layers were burnt at 450 °C during 20 min in air. The infiltration step can be repeated to increase the infiltration loading. After optimization, it was fixed to 4 steps, which gave a loading of infiltrated GDC of roughly 30 wt.% of the pre-sintered layer, as determined by mass difference before and after infiltration. The porosity of the pre-sintered layers was estimated to be around 50 %: such a loading brings the residual porosity to roughly 20 %, which is easier to eliminate during the final sintering step.

2.3 Dilatometry measurements

The dilatometry measurements were carried out using a horizontal dilatometer (Netzsch® 402 ED). Sintering experiments were performed in air on green pellets of the materials, from room temperature up to 1450 °C, with a heating rate of 5 °C/min.

2.4 SEM observations

Images of the various microstructures were recorded using a thermo-ionic gun scanning electron microscope Jeol JSM 6330 A, at an acceleration voltage of 8 kV. Prior to analyses, the samples were covered with a thin sputtered gold layer to avoid electron charging. Then, the samples were fractured and micrographs were taken on a cross section.

2.5 Electrochemical characterizations

The symmetrical cells were placed between two gold grids supported by channeled ceramics that enhance the gas diffusion toward active sites of the electrodes. Impedance spectroscopy diagrams were recorded every 50 °C between 600 °C and 400 °C at i_{dc} = 0 A·cm^{-2} with a Solartron Modulab frequency response analyzer. The frequency range was 1 MHz – 10 mHz for 400 °C and 450 °C, while above 500 °C the low frequency limit was 100 mHz. The good quality of the recorded diagrams was systematically controlled with a Kramers-Kronig test run with an in-house software (CANELEIS®). The AC amplitude was 50 mV.

The complete single cells were mounted in a dedicated measurement setup, with Ni foam as anode current collector, gold grid as cathode current collector. Air (500 NmL·min^{-1}·cm^{-2}) and 3 % wet hydrogen (250 NmL·min^{-1}·cm^{-2}) gas were supplied at each side of the cell. The setup was not sealed for gas tightness, the excess of gas being burnt at the edges.

3 Results

First, the microstructures of the GDC layers are characterized to compare the influence of the preparation method on their densification. Secondly, the electrochemical behavior of the corresponding

symmetrical cells is presented. Finally, an optimized GDC layer is prepared and its benefit characterized in a single cell configuration.

3.1 Influence of the preparation method on GDC layer densification

The microstructures of the layers prepared by both ways (sintering aids and infiltration) were characterized and compared. In the case of sintering aids, a preliminary study on GDC pellets was carried out using dilatometry measurements.

3.1.1 Sintering Aids

Figure 2 compares the sintering behavior of the GDC powder without any additive, then adding 3 % of Li, Cu or Zn. The addition of sintering aids considerably reduces the sintering temperature of GDC: considering the maximum of the sintering rate as the sintering temperature, its value decreases from 1330 °C to 1080 °C (with 3 % Zn), 950 °C (with 3 % Cu), and 930 °C (with 3 % Li). One can also note that the Li containing sample is almost fully densified (d > 95 %) at 1000°C while the Zn containing pellet only reaches 90 % of relative density at 1250 °C and the pure GDC needs 1450°C to reach the same level. Surprisingly, with Zn and Cu additive a significant decrease of the relative density (de-densification) is observed at high temperature.

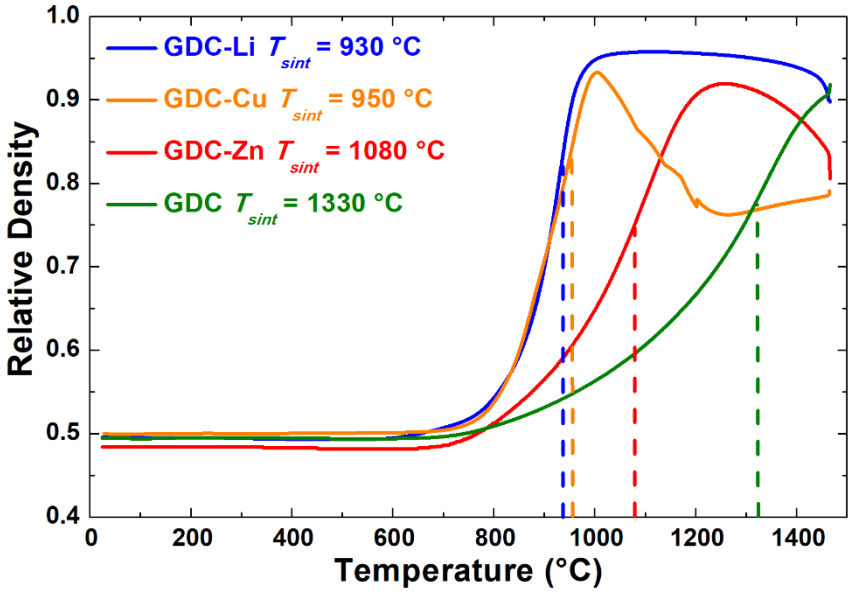

Figure 2: Sintering curves of GDC green pellets without additive and with 3 at. % of Li, Cu, or Zn

De-densification phenomena have been observed in many ceramics materials such as ZnO [31, 32], Fe_2O_3 [33], (La,Sr)FeO_3 [34-36] or $BaTiO_3$ [37-43]. One of the mechanisms most often proposed is related to the formation of a gas phase and its entrapment in the pores during the third stage of the sintering, *i.e.*

after closing of the porosity (around 90-94 % of relative density). This can also be considered for GDC-Zn and GDC-Cu. In GDC-Zn, Zn oxide present in the GDC pellet promotes the densification up to a sintered relative density of 92 % at around 1225 °C (Fig. 2). ZnO is known to decompose rapidly at temperatures above 1350 °C [44], which means that the decomposition to $Zn_{(g)}$ and ½ $O_{2(g)}$ can be observed even at lower temperatures. Then, as the temperature is increasing, ZnO evaporates in the closed pores, resulting in pore volume increase and de-densification. In GDC-Cu, the presence of CuO strongly accelerate the densification, which suggest a liquid phase mechanism. Such a mechanism is consistent with the coarsening of the microstructure (exaggerated grain growth and pore rounding) [45] as it is observed on Fig. 3. Such a microstructural evolution due to liquid phase sintering has already been observed in the case of the swelling of (La,Sr)FeO_3 ceramics [34-36]. Then, once the relative density reaches 92 % around 1000 °C, the porosity is closing. However, in the same temperature range, the CuO reduction can take place ($CuO \rightarrow Cu_2O + ½ O_2$). According to Cu-O thermodynamic data [46], the reduction of CuO under air ($p(O_2)$ = 0.2 bar) occurs at T ~ 1050 °C. Therefore, O_2 release takes place within closed pores, leading to the observed de-densification phenomenon.

To sinter the GDC layers prepared by screen printing, two strategies were considered: to sinter either at 1250 °C, which is the highest temperature that can be achieved without occurrence of the detrimental reaction between ceria and zirconia (determined in the frame of the European project ENDURANCE), or at the sintering temperature deduced from the dilatometry measurements. As the LSCF electrode must be subsequently sintered at 1050 °C, both GDC-Li and GDC-Cu layers will endure a sintering temperature higher than those determined by dilatometry. Thus, GDC-Li and GDC-Cu layers were sintered at 1050 °C, while GDC-Zn layers at 1080 °C. A reference layer was also prepared with pure GDC (without additive) and sintered at 1250 °C for 3 h. Table 1 gathers all the prepared samples, along with their sintering aid and sintering temperature. A qualitative measurement of the adhesion between zirconia, ceria, and the electrode is also reported. Unfortunately, four preparation conditions out of seven led to a delamination of the electrode. For instance, the Li addition, although strongly decreasing the sintering temperature of pellets, induces a detrimental mechanical effect leading to a systematic delamination of the electrode. Surprisingly, even for the pure GDC layer, a delamination of the electrode occurs. Even though such an architecture is well-known in literature, slight differences in the morphology of the starting GDC and LSCF powders could strongly affect the compatibility between these two materials for a given preparation protocol. For the Zn addition, only the layer sintered at 1080 °C resulted in a delamination of the electrode, whereas sintering at 1250 °C ensured a good adhesion of the whole assembly, as controlled with a tape test. Both layers prepared with GDC-Cu led to a good adhesion of the electrode.

Table 1 : Summary of the preparation conditions of the various GDC layers.

Name	Additive	Sintering treatment	Adhesion
reference	none	1250 °C 3 h	poor
GDC-Li-1050	Li 3 %	1050 °C 3 h	poor
GDC-Li-1250	Li 3 %	1250 °C 3 h	poor
GDC-Zn-1080	Zn 3 %	1080 °C 3 h	poor
GDC-Zn-1250	Zn 3 %	1250 °C 3 h	good
GDC-Cu-1050	Cu 3 %	1050 °C 3 h	good
GDC-Cu-1250	Cu 3 %	1250 °C 3 h	good

Regardless of adhesion issues, the morphology of each layer was analyzed by scanning electron microscopy to control whether the addition of Li, Zn, or Cu affects their microstructure or not. Figure 3 shows the SEM cross-section of the GDC layers depending on the additives and sintering treatment. Despite a substantial decrease of the sintering temperature of the GDC pellets from 1330 °C down to 930 °C, the Li addition (Figure 3b and c) does not improve the densification of screen-printed layers, regardless of their sintering temperature (1050 °C or 1250 °C).

On the contrary, the Zn addition (Figure 3d and e) allows a better densification than for pure GDC, however the density of the layers does not seem to be enough to prevent the surface diffusion of Sr from the cathode to the electrolyte (open porosity). As for Li addition, there is no significant difference in density between the layers treated at 1080 °C or 1250 °C, although one led to delamination while the other one led to good adhesion. Moreover, the de-densification observed by dilatometry on pellets is not significant in the case of screen printed layers. Additionally, for Zn addition, increasing the sintering time up to 10 h at 1080 °C (not shown) does not modify the densification, meaning that 3 h are sufficient.

The addition of Cu (Figure 3f and g) led to significant grain growth, but the porosity of the layer remained very high, resulting in an increase of the grains and pore size, accordingly. At low temperature (1050 °C), the layer seems denser than after a treatment at 1250 °C for 3 h, but grains are in fact just more coarsened at 1250 °C, which induces the enlargement of the pore size.

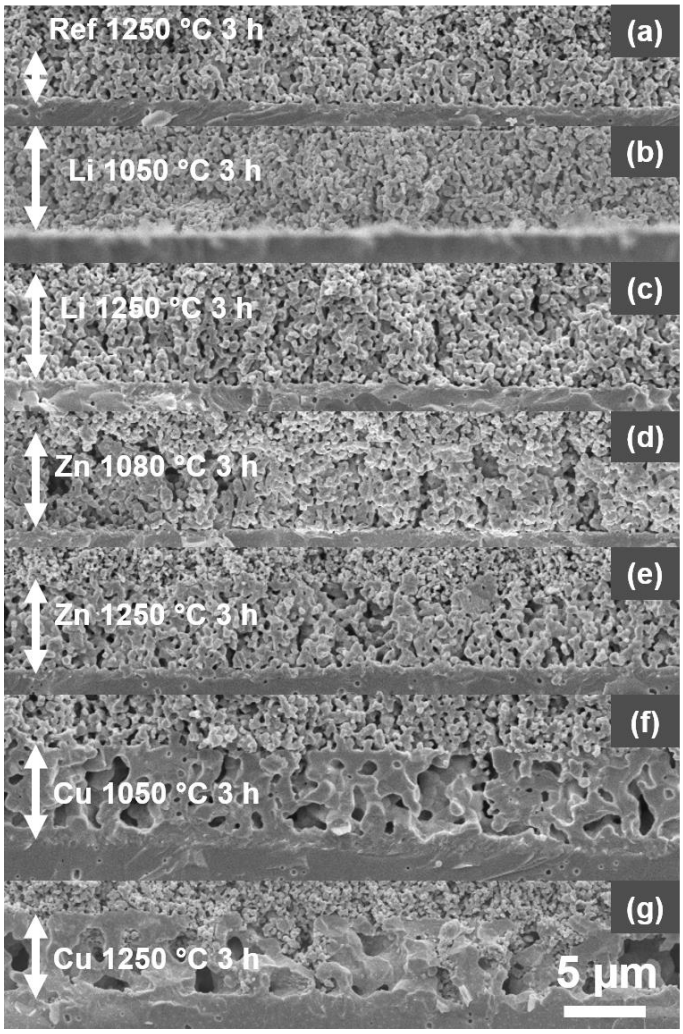

Figure 3 : SEM cross section micrographs of the GDC layers: (a) without additive, (b, c) with Li, (d, e) Zn, and (f, g) Cu additives.

The main conclusion of the morphology study is that the densification behavior of the screen-printed layers cannot be anticipated using the preliminary work performed on the corresponding pellets. Three hypotheses could explain such behavior: *i)* the limitation of the layer shrinkage because of the dense YSZ membrane beneath the layer, resulting in constrained sintering along the lateral directions. This phenomenon is known and has been reported previously [47-49]. Then, the shrinkage of the layer would be only possible along the top to bottom direction, while for pellets the shrinkage is isotropic; *ii)* a higher porosity of green screen-printed layers (compared to green pellets) would limit the densification and *iii)* the presence of organic compounds in the inks would limit the sintering aids action.

3.1.2 Infiltration process

The shrinkage issue seems then difficult to solve if the layer is only prepared by the conventional screen-printing route, even using sintering aids. An alternative way for densifying the GDC layer was

investigated in this work: the infiltration of a nitrate solution into the remaining pores of a pre-sintered screen-printed layer to fill them as much as possible before the final sintering step.

The densification of GDC layers by infiltration was considered using two GDC starting powders: with or without Cu as additive (as Cu led to the highest densification in the above section). The main goal of using GDC-Cu was to create a synergetic effect between the sintering aid and the infiltration process. The pre-sintering steps were performed at 1150 °C for pure GDC and 800 °C for GDC-Cu; they have been chosen after optimization to ensure good mechanical strength to withstand the following infiltration steps (a pre-sintering step at low temperature allows a better final density of the layer). Figure 4 shows the SEM cross section images of both samples after the pre-sintering step (a and c) and after the infiltration followed by a final sintering step at 1250 °C for 3 h (b and d).

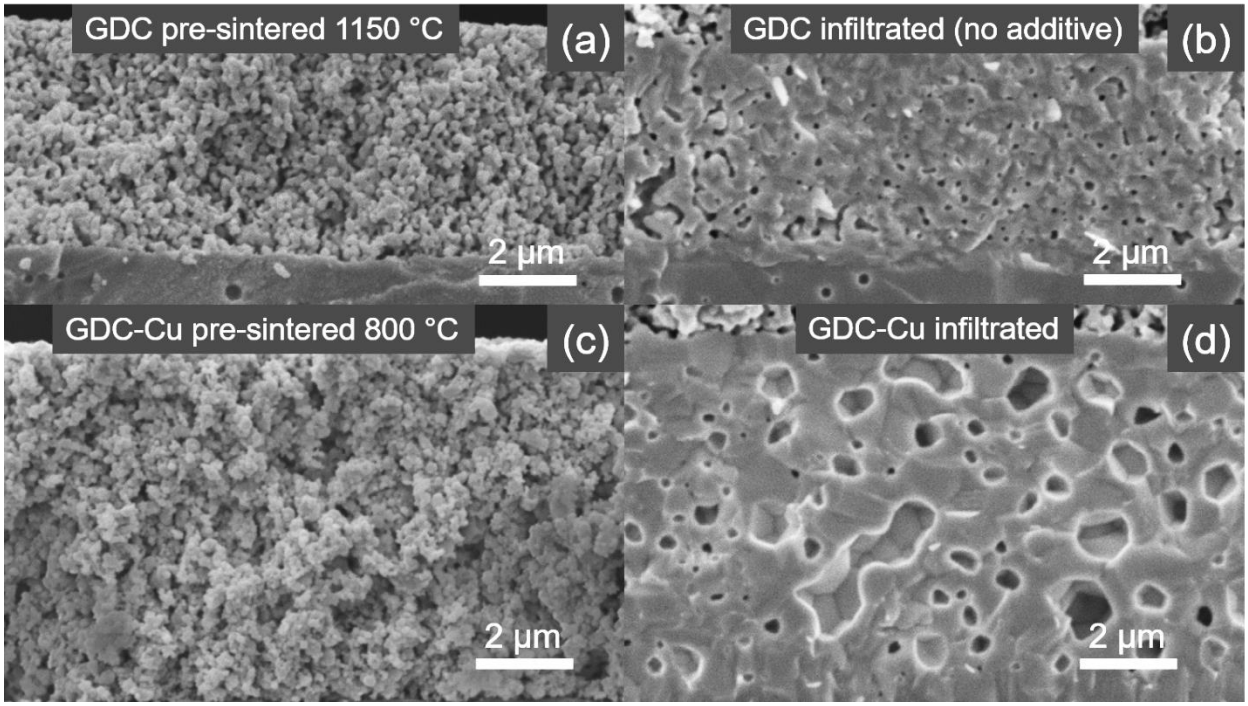

Figure 4 : SEM cross section micrographs of the GDC layers: (a) without additive pre-sintered at 1150 °C for 1 h, (b) without additive infiltrated and sintered at 1250 °C for 3 h, (c) with Cu addition pre-sintered at 800 °C for 1 h, and (d) with Cu addition infiltrated and sintered at 1250 °C for 3 h (scale bars for all four images).

The layer prepared without additive appears to be the densest layer of this study, with only few closed pores remaining (Fig. 4b). Surprisingly, the layer prepared using GDC-Cu is less dense than that prepared without additive. The expected synergetic effect does not take place, on the contrary the Cu addition seems to create additional “bubble” shaped porosity. The latter could result from the melting of some Cu based species. Indeed, the Cu-oxygen binary diagram [46] shows only liquid phases above 1230 °C. As mentioned above, the bubbles likely result from the reduction of CuO into Cu_2O at elevated temperatures, creating trapped gaseous oxygen in the closed porosity of the layer. Additionally, a very good

adhesion of the LSCF electrode screen-printed (sintered afterward) is observed on both infiltrated GDC layers.

The microstructures of the GDC layers have been successfully characterized, and both preparation methods (sintering aids addition and infiltration) led to a wide variety of GDC microstructures: the infiltration technique unambiguously produces the layers with the highest density and thus, seems to be the most promising route for the preparation of GDC interlayers. The next step of this study was the characterization of the electrochemical behavior of the oxygen electrode as a function of the preparation method.

3.2 Influence of the GDC preparation on the electrochemical performance of the electrode

The GDC layers labelled reference, GDC-Li-1050, GDC-Li-1250 and GDC-Zn-1080 (Table 1) were not considered for the electrochemical measurements, because of the adhesion issues.

Symmetrical cells including GDC-Cu-1050, GDC-Cu-1250, GDC-Zn-1250, infiltrated GDC and infiltrated GDC-Cu, were measured by impedance spectroscopy to determine their series and polarization resistance values. Because the GDC layer is located in between the electrode and the electrolyte, it is expected that the preparation protocol of this layer could influence either the contributions related to the electrolyte (series resistance, R_s) or to the LSCF electrode (polarization resistance, R_p), depending on the position of the electrical double layer [50]. To provide a clear and thorough comparison of both R_s and R_p for all the measured symmetrical cells, reference cells have first been studied.

3.2.1 Measurements of reference cells

The series resistances of each cell should match those calculated from the ionic conductivity and geometrical characteristics of their YSZ membrane, if there is no detrimental reactivity between YSZ, GDC and LSCF. The ionic conductivity of the commercial 8YSZ membranes was measured by impedance spectroscopy on a YSZ/Pt symmetrical cell. The platinum electrodes were screen-printed and sintered at 900 °C for 1 h. The reference polarization resistance of a LSCF electrode was measured on a cell based on a GDC electrolyte, because the reactivity between YSZ and LSCF will affect the polarization resistance, whereas GDC is a compatible electrolyte for LSCF electrodes. LSCF was prepared using the same conditions as mentioned above (screen-printing and sintering at 1050 °C for 1 h). A typical diagram of the GDC/LSCF reference cell is available in SI1. Table 2 gathers the YSZ conductivity (corresponding to the R_s of the YSZ/Pt cell) and LSCF polarization resistance values in the 400 - 700 °C temperature range. These values will be further considered as lower limit for R_s and R_p and any deviation from them for all the measured symmetrical cells will be considered as a result of a degradation caused by the preparation of the GDC interlayer, which is the only changing parameter among all cells.

Table 2: Reference values of the ionic conductivity, σ_i of YSZ (measured on YSZ/Pt cell) and of the polarization resistance, R_p, of the LSCF electrode (measured on a GDC/LSCF cell).

Temperature (°C)	$\sigma_{i\ YSZ}$ ($S \cdot cm^{-1}$) YSZ/Pt cell	$R_{p\ LSCF}$ ($\Omega \cdot cm^2$) GDC/LSCF cell
400	1.42×10^{-4}	22.7
450	4.63×10^{-4}	4.46
500	1.33×10^{-3}	1.06
550	3.17×10^{-3}	0.33
600	6.77×10^{-3}	0.12
650	1.30×10^{-2}	0.06
700	2.16×10^{-2}	0.03

3.2.2 Symmetrical cells

Symmetrical cells including various GDC interlayers were measured by impedance spectroscopy between 700 °C and 400 °C. Figure 5 compares their impedance diagrams. At 500 °C, the diagrams mainly consist in two contributions, except for the cell with a GDC-Cu layer sintered at 1050 °C, which exhibits an additional contribution located between the two others. The high frequency contribution ($f > 10^4$ Hz) is related to the O^{2-} diffusion at the grain boundaries of the electrolyte [51]. Its magnitude strongly varies from one cell to another, showing that the grain boundary contribution is dependent on the GDC interlayer nature. Indeed, GDC being a pure ionic conductor, it is also part of the electrolyte, therefore the grain boundaries within the GDC layer or at the YSZ/GDC interface also contribute to the O^{2-} diffusion. The cells prepared with the infiltrated GDC layer shows the smallest grain boundary contribution, whereas the cell prepared with GDC-Cu sintered at 1050 °C shows the largest one.

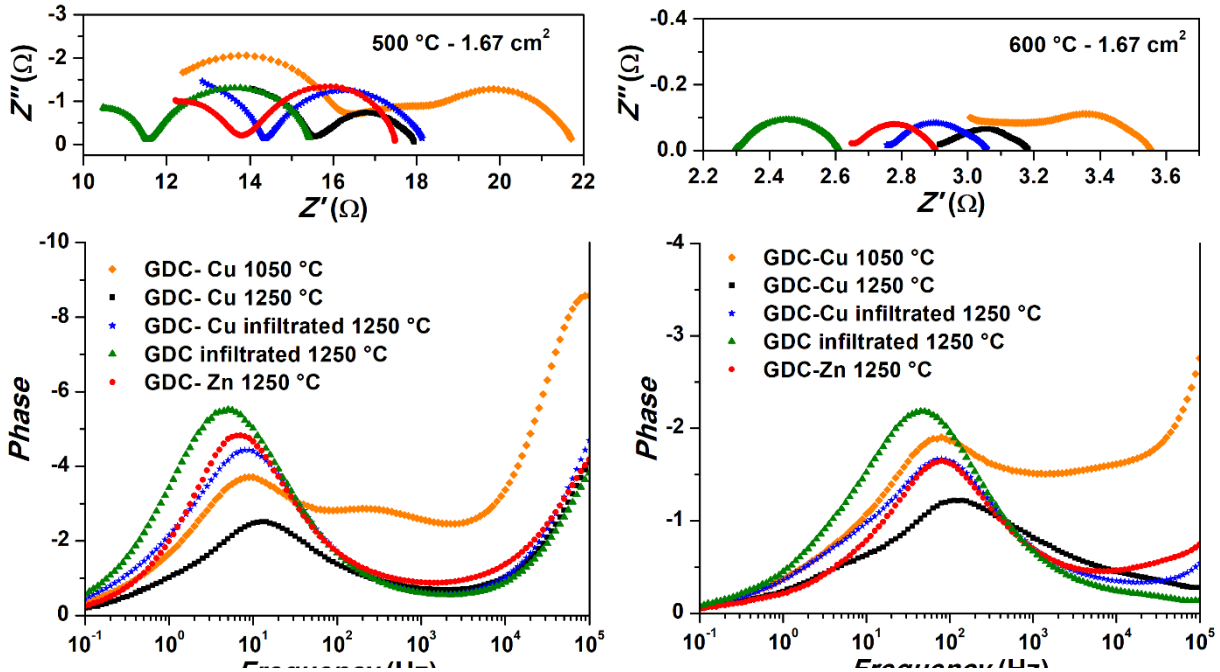

Figure 5: Impedance diagrams of the various LSCF/GDC/YSZ/GDC/LSCF symmetrical cells recorded at 500 °C and 600 °C (the area of the cells is 1.67 cm^2).

The additional contribution located at mid-frequency (10^2 Hz < f < 10^3 Hz at 500 °C) in the case of GDC-Cu sintered at 1050 °C suggests that this specific layer probably induces transfer limitations at the GDC/LSCF interface where the electrical double layer is located; therefore, the resistance associated with this phenomenon increases. Possible assumption can be a low contact area between the GDC and LSCF grains, or the formation of a detrimental interphase, resulting from the presence of Cu. Such a contribution does not appear on the diagrams of the other cells, suggesting that in these cases the resistance associated with the double layer is low enough not to limit the cell performance.

The low frequency contribution (1 Hz < f < 10 Hz at 500 °C) is related to the oxygen electrode reaction [51]; it is rather similar for all cells except for the one prepared with a GDC-Cu layer sintered at 1250 °C, for which the contribution is smaller. Such similarities would suggest that the GDC interlayer has a stronger influence on the series resistance (related to the pure ionic conductive area of the cell) than it has on the polarization resistance (related to the mixed conductive area of the cell provided by the LSCF electrodes).

To clearly visualize the influence of the GDC layer, both R_s and R_p values measured on both YSZ/Pt and GDC/LSCF reference cells (Table 2) were subtracted to those measured for each YSZ/GDC/LSCF symmetrical cells. It allowed determining ΔR_s and ΔR_p values at 400 °C, 500 °C, and 600 °C, which are plotted in Figure 6. The polarization resistance is higher than that of the reference GDC/LSCF cell whatever

the preparation conditions of the GDC interlayer, suggesting that the optimization of the GDC preparation is still not fully achieved. The dispersion of ΔR_p values between all cells is rather large at 400 °C, but become narrower when increasing the measurement temperature. At 600 °C all ΔR_p values are similar except for the cell prepared with GDC-Cu sintered at 1050 °C, of which difference is due to the presence of the already quoted additional interfacial contribution (Figure 5), which is included in the total R_p. Those similarities suggest that the polarization resistance values are not directly related to the density of the GDC interlayer. Preferably, a careful attention must be taken on the reactivity between both layers, which can form detrimental phases. Indeed, Irvine *et al.* already discussed the paramount importance of interfaces in the performance of electrochemical devices such as SOFC or electrolyzers [52].

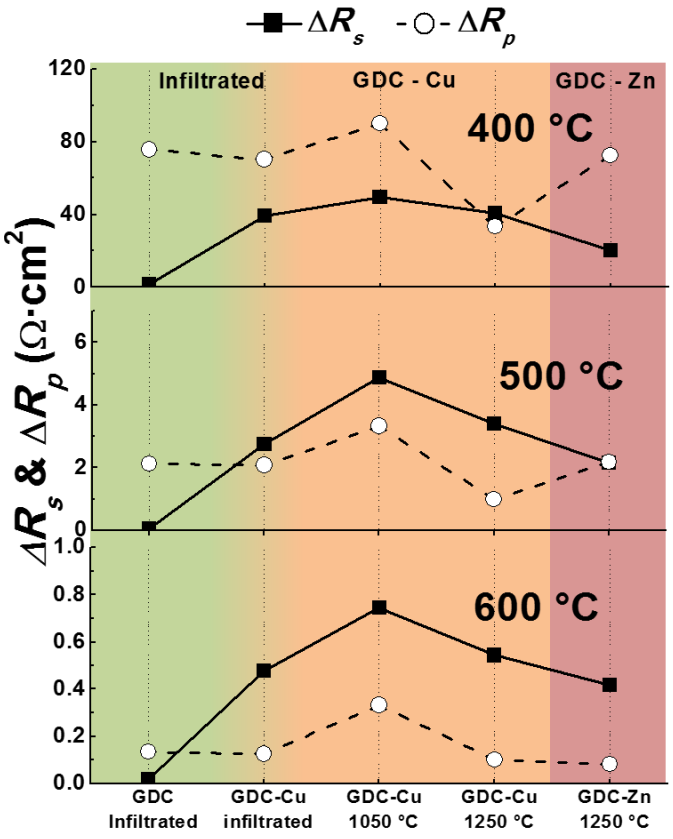

Figure 6: Comparison of ΔR_s (filled squares – solid line) and ΔR_p (hollow circles – dashed line) at 400 °C, 500 °C and 600 °C for all cells, depending on the preparation method of the GDC interlayer. The values for the cells prepared with GDC-Zn sintered at 1080 °C are not represented because the electrode was partially delaminated after the measurements.

The series resistances strongly depend on the considered layer. The infiltrated GDC layer prepared without sintering aid leads to a ΔR_s value close to zero at all temperatures, meaning that no detrimental phase that could block the ionic diffusion is formed at the GDC/YSZ interface. For all cells prepared with a sintering aid in the GDC powder, the additional series resistance ΔR_s is rather large. Even though ΔR_s induced by GDC-Zn is still significant, the Zn addition seems less damageable for the series resistance than the Cu addition. Indeed, the three cells prepared with GDC-Cu starting powder show the highest ΔR_s,

regardless of their density. The sintering temperature of GDC-Cu plays an important role on the ΔR_s value but not in the expected manner. Indeed, the layer sintered at low temperature (1050 °C) leads to higher ΔR_s value, whereas both GDC-Cu layers sintered at 1250 °C (infiltrated and not infiltrated) exhibit the same ΔR_s. If the additional resistance comes from a chemical reactivity between YSZ and GDC, then ΔR_s should increase with the sintering temperature. The opposite trend is observed. However, if the reactivity is correlated with the presence of Cu, then its possible evaporation at 1250 °C, as suggested in part 3.1.2, may explain why GDC layers are less reactive when sintered at 1250 °C rather than at 1050 °C, as a higher amount of Cu should remain in the layer. Chemical analyses of the interfaces by SEM/EDS do not bring any valuable information on the interface/interphase compositions because of its rather low resolution. A careful study with higher resolution tools such as TEM would be valuable to further support these observations. One could also think that the sintering aids can affect the conductivity of GDC, therefore increasing R_s. However, as shown by Nicholas and De Jonghe [18], the addition of sintering elements into GDC can only affect the conductivity positively, so the additional R_s cannot be explained by the sole resistance of the prepared GDC layer.

Our study points out a key aspect concerning the use of sintering aids for improving the densification of GDC interlayers. The addition of metal species significantly enhances the sintering between GDC grains, and such enhancement is likely due to a modification of their surface chemistry that could lower the energy barrier to initiate the sintering process. The modification of the GDC grains surface reactivity decreases the sintering temperature of GDC, but this improvement comes with a major drawback: as the surface reactivity of GDC grains increases, the reactivity between GDC and YSZ increases as well. Then the formation of detrimental interphases may start at lower temperature for a GDC powder with sintering aids than it does for pure GDC powder.

Sintering aids were initially considered for densifying GDC at lower temperature to avoid the reaction with YSZ. But the results reported here clearly show that the benefit brought by the sintering aids in terms of a decrease of the sintering temperature is completely counter-balanced by the increase of the chemical reactivity with YSZ, thus bringing back the initial problem encountered with pure GDC at higher temperature. Then, using sintering aids may not be the optimal way to prepare dense GDC interlayers.

We suggest that the densification of GDC by infiltration of Ce/Gd solution without additional element is a very promising method, as it produces dense interlayers without increasing the series resistance of the cell. To validate the results obtained on symmetrical cells, the infiltrated GDC interlayer was integrated into a single cell, whose performance was measured.

3.2.3 *Complete Single Cell measurements*

A single cell containing infiltrated GDC layer was prepared using a commercial Ni-YSZ/YSZ half-cell, following the same protocol as for symmetrical cells. For comparison, a single cell using a commercial half-cell that already contains the GDC interlayer was also prepared. Figure 7 shows the *i-V* curves and impedance diagrams measured on both cells at 700 °C and 800 °C.

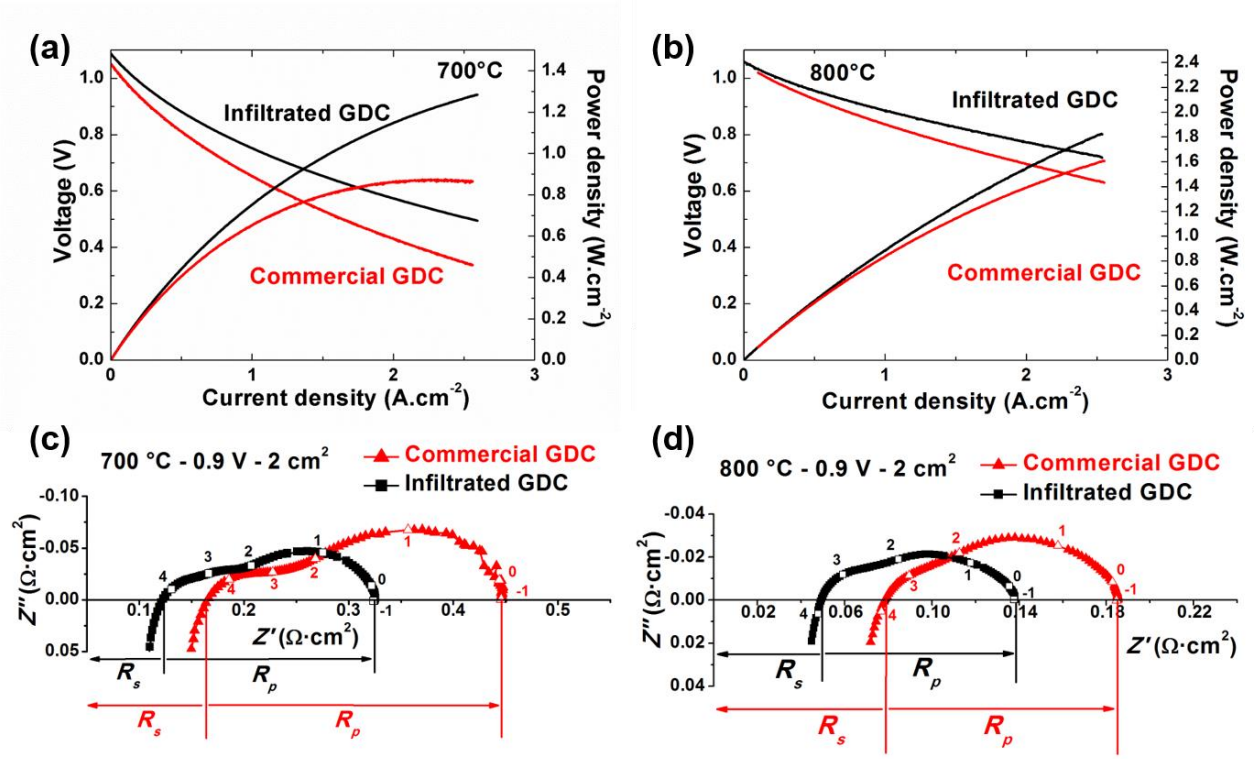

Figure 7: *i-V* curves and power densities recorded on single cells (active area = 2 cm^2) using infiltrated and commercial GDC at (a) 700 °C and (b) 800 °C; corresponding impedance diagrams recorded at 0.9 V at (c) 700 °C and (d) 800 °C.

The cell containing the infiltrated GDC layer shows a substantially higher performance than the commercial one, the power density at 0.7 V being increased from 0.59 W·cm^{-2} up to 0.87 W·cm^{-2} at 700 °C, and from 1.30 W·cm^{-2} up to 1.82 W·cm^{-2} at 800 °C. This corresponds to a performance gain of 40-50 % just by changing the GDC interlayer. The maximum power density goes up to more than 1.3 W·cm^{-2} at 700 °C and can probably reach 2 W·cm^{-2} at 800 °C (experiments are limited by our set-up capabilities, $I \leq$ 2.5 A·cm^{-2}). Such an improvement in the cell performance is consistent with the results reported by Choi *et al.* on cells with GDC interlayers infiltrated with a sol of GDC [30]. Although the results of both studies are similar, the preparation technique presented here is simpler and requires less steps, which could make it more interesting from an industrial standpoint. Therefore, densifying the GDC interlayer by nitrate infiltration is a highly promising method.

The impedance diagrams recorded at 0.9 V (Figure 7 c and d) for both cells and at both temperatures allow understanding the origin of such performance improvement. At 700 °C, both R_s and R_p are lower for the infiltrated GDC cell, whereas at 800 °C the main benefits come from the R_s decrease. Indeed, as the electrode kinetics are faster at sufficiently high temperature, the ohmic loss in the electrolyte becomes the limiting factor.

The decrease of series resistance observed using the infiltrated GDC layer agrees with the results here obtained on symmetrical cells (part 3.2.2), clearly pointing out that limiting the GDC/YSZ reactivity is mandatory to improve the cell performance. The comparison of SEM cross-section images of both cells (Figure 8) further supports this observation. On the cell prepared with a commercial GDC layer the back-scattered image (Figure 8d) highlights an inter-diffusion layer between GDC and YSZ. Such inter-diffusion layer probably corresponds to the formation of interphases with lower ionic conductivity resulting in an increase in series resistance [13]. On the cell prepared with an infiltrated GDC interlayer, the inter-diffusion layer is hardly visible, which is consistent with the lower R_s values. Moreover, the GDC/YSZ bi-layer is thicker in the cell with infiltrated GDC (≈ 8 µm) than in the cell with commercial GDC (≈ 5 µm), but the R_s is smaller anyway, which means that the interfacial reactivity between cell components has a larger impact on the resistance of the cell than their respective thicknesses.

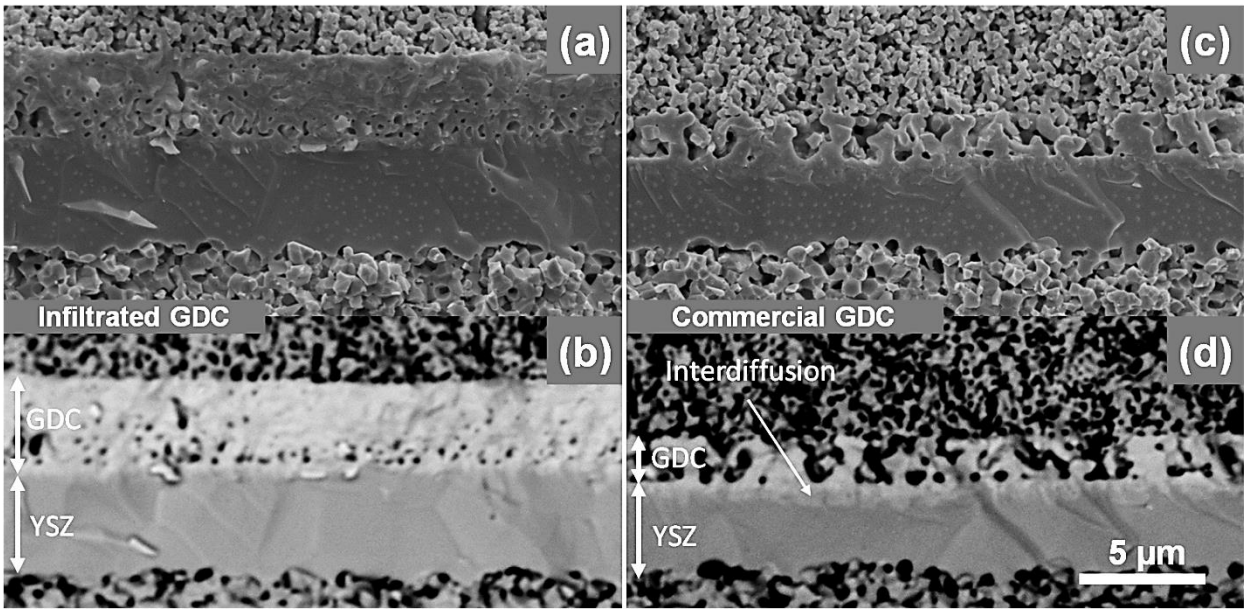

Figure 8: SEM cross section images of single cells including an infiltrated GDC layer (a, b) and a commercial GDC layer (c, d). Images (a, c) are recorded in secondary electron mode and (b, d) in back-scattered electron mode.

4 Conclusion

This study aimed to evaluate two strategies to improve the densification of the GDC interlayer used in solid oxide fuel cells, which is mandatory to limit the Sr diffusion from the electrode toward the YSZ electrolyte. Two routes were compared here: using metal nitrates in the screen-printed layers as sintering aids or densifying a porous layer by infiltration. The action of sintering aids has first been evidenced by dilatometry measurements performed on pellets, then by SEM on screen-printed layers. The infiltration technique was applied on pre-sintered screen-printed layers. Both ways were evaluated in terms of microstructure of the layer and of electrochemical compatibility with the YSZ electrolyte and LSCF electrode. The main features highlighted here are:

1) The sintering behavior of GDC pellets characterized by dilatometry is very different from the sintering behavior of screen-printed layers.
2) Among Li, Zn, and Cu, the Cu addition leads to the highest densification of screen-printed layers, but the shrinkage of the layers is mechanically constrained by the YSZ support.
3) Using sintering aids results in an enhanced reactivity of the GDC layers with the YSZ electrolyte, ultimately leading to large increase of the series resistances due to the formation of detrimental phases at the GDC/YSZ interface.
4) The infiltration of Ce and Gd nitrates into pre-sintered porous GDC layers produces highly dense layers, showing that this way is a very promising route for densifying GDC interlayers.
5) The infiltration route substantially limits the chemical reactivity between GDC and YSZ as compared to using sintering aids, which considerably limits the occurrence of additional series resistances.
6) The single cell prepared with an infiltrated GDC interlayers exhibits performance 40 to 50 % higher than that prepared with commercial GDC layers.

5 Acknowledgments

The research leading to these results has received funding from the European Union's Seventh Framework Programme (FP7/2007-2013) Fuel Cells and Hydrogen Joint Undertaking (FCU-JU-2013-1) under grant agreement No 621207. The authors would like to acknowledge the ENDURANCE consortium for fruitful discussions.

6 References

[1] H. Tu, Y. Takeda, N. Imanishi, O. Yamamoto, $Ln_{0.4}Sr_{0.6}Co_{0.8}Fe_{0.2}O_{3-\delta}$ (Ln=La, Pr, Nd, Sm, Gd) for the electrode in solid oxide fuel cells, Solid State Ionics 117 (3-4) (1999) 277–281.

[2] A. Mai, V. Haanappel, F. Tietz, D. Stöver, Ferrite-based perovskites as cathode materials for anode-supported solid oxide fuel cells. part ii. influence of the CGO interlayer, Solid State Ionics 177 (19-25 SPEC. ISS.) (2006) 2103–2107.

[3] G. Constantin, C. Rossignol, P. Briois, A. Billard, L. Dessemond, E. Djurado, Efficiency of a dense thin CGO buffer layer for solid oxide fuel cell operating at intermediate temperature, Solid State Ionics 249-250 (2013) 98–104.

[4] V. Wilde, H. Störmer, J. Szász, F. Wankmüller, E. Ivers-Tiffée, D. Gerthsen, Effect of $Gd_{0.2}Ce_{0.8}O_2$ sintering temperature on formation of a $SrZrO_3$ blocking layer between $Y_{0.16}Zr_{0.84}O_2$, $Gd_{0.2}Ce_{0.8}O_2$ and $La_{0.58}Sr_{0.4}Co_{0.2}Fe_{0.8}O_3$, Vol. 66, 2015, pp. 103–107.

[5] S. Uhlenbruck, N. Jordan, D. Sebold, H. Buchkremer, V. Haanappel, D. Stöver, Thin film coating technologies of $(Ce,Gd)O_{2-\delta}$ interlayers for application in ceramic high-temperature fuel cells, Thin Solid Films 515 (7-8) (2007) 4053–4060.

[6] S. Uhlenbruck, T. Moskalewicz, N. Jordan, H.-J. Penkalla, H. Buchkremer, Element interdiffusion at electrolyte-cathode interfaces in ceramic high-temperature fuel cells, Solid State Ionics 180 (4-5) (2009) 418–423.

[7] D. Szymczewska, A. Chrzan, J. Karczewski, S. Molin, P. Jasinski, Spray pyrolysis of doped-ceria barrier layers for solid oxide fuel cells, Surf. Coat. Technol. 313 (2017) 168–176.

[8] J. Szasz, F. Wankmüller, V. Wilde, H. Störmer, D. Gerthsen, N. Menzler, E. Ivers-Tiffée, Nature and functionality of oxygen/cathode/electrolyte-interfaces in SOFCs, in: ECS Transactions, Vol. 66, 2015, pp. 79–87.

[9] J.-H. Song, M. Jung, H. Park, H.-T. Lim, The effect of fabrication conditions for GDC buffer layer on electrochemical performance of solid oxide fuel cells, Nano-Micro Letters 5 (3) (2013) 151–158.

[10] N. Jordan, W. Assenmacher, S. Uhlenbruck, V. Haanappel, H. Buchkremer, D. Stöver, W. Mader, Ce $Gd_{0.2}O_{2-\delta}$ protecting layers manufactured by physical vapor deposition for IT-SOFC, Solid State Ionics 179 (21-26) (2008) 919–923.

[11] P. Hjalmarsson, M. Søgaard, M. Mogensen, Electrochemical performance and degradation of $(La_{0.6}Sr_{0.4})_{0.99}CoO_{3-\delta}$ as porous SOFC-cathode, Solid State Ionics 179 (27-32) (2008) 1422–1426.

[12] F. Wang, M. Nishi, M. Brito, H. Kishimoto, K. Yamaji, H. Yokokawa, T. Horita, Sr and Zr diffusion in LSCF/10GDC/8YSZ triplets for solid oxide fuel cells (SOFCs), J. Power Sources 258 (2014) 281–289.

[13] T. Matsui, S. Li, H. Muroyama, K. Kishida, H. Inui, K. Eguchi, Electrochemical property of solid solutions formed in (La,Sr)(Co,Fe)$O_{3-\delta}$ cathode/doped-CeO_2 interlayer/Y_2O_3-ZrO_2 electrolyte system during operation of solid oxide fuel cells, Solid State Ionics 300 (2017) 135–139.

[14] A. Tsoga, A. Gupta, A. Naoumidis, P. Nikolopoulos, Gadolinia-doped ceria and yttria stabilized zirconia interfaces: Regarding their application for SOFC technology, Acta Mater. 48 (2000) 4709–4714.

[15] A. Tsoga, A. Naoumidis, D. Stöver, Total electrical conductivity and defect structure of ZrO_2-CeO_2-Y_2O_3-Gd_2O_3 solid solutions, Solid State Ionics 135 (1-4) (2000) 403–409.

[16] J.-J. Choi, D.-S. Park, B.-G. Seong, H.-Y. Bae, Low-temperature preparation of dense (Gd,Ce)$O_{2-\delta}$-Gd_2O_3 composite buffer layer by aerosol deposition for YSZ electrolyte-based SOFC, Int. J. Hydrogen Energy 37 (12) (2012) 9809–9815.

[17] Y. Gong, W. Ji, L. Zhang, M. Li, B. Xie, H. Wang, Y. Jiang, Y. Song, Low temperature deposited (Ce,Gd)O_{2-x} interlayer for $La_{0.6}Sr_{0.4}Co_{0.2}Fe_{0.8}O_3$ cathode based solid oxide fuel cell, J. Power Sources 196 (5) (2011) 2768 – 2772.

[18] J. Nicholas, L. De Jonghe, Prediction and evaluation of sintering aids for cerium gadolinium oxide, Solid State Ionics 178 (2007) 1187–1194.

[19] H. Yoshida, K. Miura, J.-I. Fujita, T. Inagaki, Effect of gallia addition on the sintering behavior of samaria-doped ceria, J. Am. Ceram. Soc. 82 (1) (1999) 219–221.

[20] Y. Kang, G. Choi, The effect of alumina and Cu addition on the electrical properties and the SOFC performance of Gd-doped CeO_2 electrolyte, Solid State Ionics 180 (11-13) (2009) 886–890.

[21] C. Kleinlogel, L. Gauckler, Sintering and properties of nanosized ceria solid solutions, Solid State Ionics 135 (1-4) (2000) 567–573.

[22] D. Pérez-Coll, P. Núñez, J. Abrantes, D. Fagg, V. Kharton, J. Frade, Effects of firing conditions and addition of Co on bulk and grain boundary properties of CGO, Solid State Ionics 176 (37-38) (2005) 2799–2805.

[23] L. Villas-Boas, P. De Paula Nascente, R. Landers, M. Campos, D. De Souza, The effect of Co and Zn addition on densification and electrical properties of ceria-based nanopowders, Mater. Res. 19 (5) (2016) 1057–1063.

[24] L. Villas-Boas, F. Figueiredo, D. De Souza, F. Marques, Zn as sintering aid for ceria-based electrolytes, Solid State Ionics 262 (2014) 522–525.

[25] J.-A. Lee, Y.-E. Lee, H.-C. Lee, Y.-W. Heo, J.-H. Lee, J.-J. Kim, Effect of Li_2O content and sintering temperature on the grain growth and electrical properties of Gd-doped CeO_2 ceramics, Ceram. Int. 42 (9) (2016) 11170–11176.

[26] A. K. Baral, H. P. Dasari, B.-K. Kim, J.-H. Lee, Effect of sintering aid (CoO) on transport properties of nanocrystalline Gd doped ceria (GDC) materials prepared by co-precipitation method, J. Alloys Compd. 575 (2013) 455 – 460.

[27] T. Zhang, P. Hing, H. Huang, J. Kilner, Sintering and grain growth of coo-doped ceo2 ceramics, J. Eur. Ceram. Soc. 22 (1) (2002) 27 – 34.

[28] D. Pérez-Coll, D. Marrero-López, P. Núñez, S. Piñol, J. Frade, Grain boundary conductivity of $Ce_{0.8}Ln_{0.2}O_{2-\delta}$ ceramics (Ln=Y, La, Gd, Sm) with and without Co-doping, Electrochim. Acta 51 (28) (2006) 6463 – 6469.

[29] D. Ni, V. Esposito, Densification of $Ce_{0.9}Gd_{0.1}O_{1.95}$ barrier layer by in-situ solid state reaction, J. Power Sources 266 (2014) 393–400.

[30] H.-J. Choi, Y.-H. Na, D.-W. Seo, S.-K. Woo, S.-D. Kim, Densification of gadolinia-doped ceria diffusion barriers for SOECs and IT-SOFCs by a sol-gel process, Ceram. Int. 42 (1) (2016) 545–550.

[31] A. Solomon, F. Hsu, Swelling and gas release in ZnO, Journal of the American Ceramic Society 63 (7-8) (1980) 467–474.

[32] B. Balzer, M. Hagemeister, P. Kocher, L. Gauckler, Mechanical strength and microstructure of zinc oxide varistor ceramics, Journal of the American Ceramic Society 87 (10) (2004) 1932–1938.

[33] M. Nasr, A. Omar, M. Hessien, A. El-Geassy, Carbon monoxide reduction and accompanying swelling of iron oxide compacts, ISIJ International 36 (2) (1996) 164–171.

[34] L. Sagdahl, M.-A. Einarsrud, T. Grande, Sintering of $LaFeO_3$ ceramics, Journal of the American Ceramic Society 83 (9) (2000) 2318–2320.

[35] K. Kleveland, M.-A. Einarsrud, T. Grande, Sintering behavior, microstructure, and phase composition of $Sr(Fe,Co)O_{3-\delta}$ ceramics, Journal of the American Ceramic Society 83 (12) (2000) 3158–3164.

[36] L. Sagdahl, M.-A. Einarsrud, T. Grande, Sintering behaviour of $La_{1-x}Sr_xFeO_{3-\delta}$ mixed conductors, Journal of the European Ceramic Society 26 (16) (2006) 3665–3673.

[37] M. Delfrate, J. Lemaitre, V. Buscaglia, M. Leoni, P. Nanni, Slip casting of submicron $BaTiO_3$ produced by low-temperature aqueous synthesis, Journal of the European Ceramic Society 16 (9) (1996) 975–984.

[38] M. Demartin, C. Hérard, C. Carry, J. Lemaître, Dedensification and anomalous grain growth during sintering of undoped barium titanate, Journal of the American Ceramic Society 80 (5) (1997) 1079–1084.

[39] P. Duran, J. Tartaj, C. Moure, Sintering behaviour and microstructural evolution of agglomerated spherical particles of high-purity barium titanate, Ceramics International 29 (4) (2003) 419–425.

[40] C. Hérard, A. Faivre, J. Lemaître, Surface decontamination treatments of undoped $BaTiO_3$ - part II: Influence on sintering, Journal of the European Ceramic Society 15 (2) (1995) 145–153.

[41] C. Proust, C. Miot, E. Husson, Characterization of $BaTiO_3$ powder obtained by a chemical route, Journal of the European Ceramic Society 15 (7) (1995) 631–635.

[42] B.-K. Yoon, E.-Y. Chin, S.-J. Kang, Dedensification during sintering of $BaTiO_3$ caused by the decomposition of residual $BaCO_3$, Journal of the American Ceramic Society 91 (12) (2008) 4121–4124.

[43] V. Schmitt, F. Raether, Effect of cobalt doping on the sintering mechanisms of the lead-free piezoceramic $(Bi_{0.5}Na_{0.5})TiO_3$, Journal of the European Ceramic Society 34 (1) (2014) 15–21.

[44] M. Asadian, Thermodynamic analysis of ZnO crystal growth from the melt, J. Cryst. Process Tech. 3 (2013) 75–80.

[45] R. German, Sintering Theory and Practice, John Wiley and Sons, 1996.

[46] J. Neumann, T. Zhong, Y. Chang, The Cu-O (copper-oxygen) system, Bulletin of Alloy Phase Diagrams 5 (2) (1984) 136–140.

[47] R. Bordia, R. Raj, Sintering behavior of ceramic films constrained by a rigid substrate, J. Am. Ceram. Soc. 68 (6) (1985) 287–292.

[48] D. Carroll, M. Rahaman, An initial stage model for the sintering of constrained polycrystalline thin films, J. Eur. Ceram. Soc. 14 (5) (1994) 473–479.

[49] T. Garino, H. Bowen, Kinetics of constrained-film sintering, J. Am. Ceram. Soc. 73 (2) (1990) 251–257.

[50] A. Flura, C. Nicollet, V. Vibhu, B. Zeimetz, A. Rougier, J.-M. Bassat, J.-C. Grenier, Application of the Adler-Lane-Steele model to porous $La_2NiO_{4+\delta}$ cathode for SOFC application: influence of the interface with gadolinia doped ceria, J. Electrochem. Soc. 163 (2016) F523–F532.

[51] E. Schouler, N. Mesbahi, G. Vitter, In situ study of the sintering process of yttria stabilized zirconia by impedance spectroscopy, Solid State Ionics 9-10 (PART 2) (1983) 989–996.

[52] J. Irvine, D. Neagu, C. Verbraeken, C. Chatzichristodoulou, C. Graves, M. Mogensen, Evolution of the electrochemical interface in high-temperature fuel cells and electrolysers, Nature Energy 1 (2016) 15014.

Supplementary information 1: Impedance Diagram recorded at 500 °C on the GDC/LSCF reference cell (cell area: 1.67 cm^2)